SCIENCE CHINA
Information Sciences

• RESEARCH PAPER •

September 2021, Vol. 64 192302:1–192302:12
https://doi.org/10.1007/s11432-019-2918-7

Orbital angular momentum multiplexing communication system over atmospheric turbulence with K-best detection

Yingmeng GE[1,2,3], Liang WU[2], Chuan ZHANG[1,2,3*] & Zaichen ZHANG[2,3*]

[1]*Laboratory of Efficient Architectures for Digital-communication and Signal-processing (LEADS), Southeast University, Nanjing* 211189*, China;*
[2]*National Mobile Communications Research Laboratory, Southeast University, Nanjing* 211189*, China;*
[3]*Purple Mountain Laboratories, Nanjing* 211189*, China*

Received 24 October 2019/Revised 7 February 2020/Accepted 12 May 2020/Published online 9 August 2021

Abstract As the optical communication technology advances, vortex beam with orbital angular momentum (OAM) has gained wide attention due to its potential to significantly increase the channel capacity. Under the influence of atmospheric turbulence, there are still challenging problems in the OAM multiplexing system. To the best of our knowledge, in this paper one multiple-input-multiple-output (MIMO) detection technology named K-best detection, is first applied to the OAM multiplexing system. Numerical simulation results indicate the proposed solution enhances the performance of the optical communication system compared with data-aided least mean square (DA-LMS) and minimum mean squared error (MMSE) detection. Furthermore, with MMSE sorted QR decomposition (MMSE-SQRD) preprocessing, the performance of K-best detection can be further improved. When $C_n^2 = 1\times10^{-14}$, about 4.4 dB signal-to-noise ratio (SNR) gain can be obtained by preprocessing at $k = 2$ while the complexity is not significantly increased. Computational complexity is also analyzed in this paper, results show that K-best detection with winner path extension (WPE) algorithm can achieve 43% system complexity reduction, achieving a compromise between performance and complexity in K-best detection.

Keywords orbital angular momentum, atmospheric turbulence, K-best detection, MMSE-SQRD preprocessing, WPE algorithm

Citation Ge Y M, Wu L, Zhang C, et al. Orbital angular momentum multiplexing communication system over atmospheric turbulence with K-best detection. Sci China Inf Sci, 2021, 64(9): 192302, https://doi.org/10.1007/s11432-019-2918-7

1 Introduction

Free-space optical communications (FSOCs) has gradually gained wide attention as a very important application area. Since FSOC has higher modulation bandwidth, it has higher information capacity than radio frequency (RF) communication systems [1]. Besides, the inherent high gain characteristics of laser beams [2] and the significant degrees of robustness and covertness provided by FSOC [3] afford many more benefits than RF communication systems.

To achieve a higher information capacity of FSOC systems, one can apply the multiplexing technologies, e.g., wavelength-division multiplexing (WDM) [4, 5], polarization division multiplexing (PDM) [6], and frequency division multiplexing (FDM) [7] to the system. With the development of these multiplexing technologies, it becomes more and more difficult to further improve the data transmission capacity of the FSOC systems. Recently, a new physical property that can be used in multiplexing technologies, orbital angular momentum (OAM), has gained wide attention from scientific researchers due to its unique properties [8–10]. Vortex beam is a sort of light that carries OAM, which has a hollow intensity distribution and a spiral phase front. There are many ways to generate vortex beams, including spiral phase plates [11], phase holograms [12, 13], metasurfaces [14]. The most important property of vortex beams is

* Corresponding author (email: chzhang@seu.edu.cn, zczhang@seu.edu.cn)

that vortex beams with different OAM states are orthogonal, which means OAM states can be utilized for a new multiplexing method. As a special case of space division multiplexing (SDM), the technology of OAM division multiplexing (OAM-DM) offers great potential for increasing the capacity of the FSOC system.

In recent years, optical wireless communication based on vortex beams has been rapidly developed. Gibson et al. [8] proposed a communication scheme based on OAM shift keying (OAM-SK) in 2004. Signals are encoded into eight vortex beams with different OAM states, the receiving end demodulates the signal through the forked grating. In the same year, Bouchal et al. [15] proposed a communication scheme based on OAM-DM, in which signals of different paths are multiplexed by being loaded on vortex beams with different OAM states. Djordjevic et al. [16] applied low-density parity-check (LDPC) coding in vortex optical communication and greatly reduced the error rate of OAM beams transmitted in atmospheric turbulence. Ref. [17] studied the optimal sets of OAM states under different turbulence conditions, along with the total system capacity. Wang et al. [18] combined the PDM technology with the OAM-DM technology, and use 16QAM signal modulation to achieve a spectrum utilization of 25.6 bit/s/Hz. Du et al. [19] experimentally demonstrated high-dimensional optical coding/decoding based on Bessel beams in an FSOC system and analyzed the BER performance of different coding/decoding forms and topological numbers. Refs. [20–22] provide different perspectives on the FSOC system with OAM beams in detail. OAM-DM multiplexing technologies can be combined with other multiplexing technologies to obtain a higher channel transmission rate and spectrum utilization rate, and some different signal modulation schemes can also be applied to the FSOC system.

However, one of the trickiest problems of the FSOC system is the atmospheric turbulence caused by temperature differential [2], which brings side effects on bit-error-rate (BER) performance at the demodulation end. To solve these problems, several turbulence mitigation approaches are discussed in [23], adaptive optics-based (optical domain) and signal processing-based (electrical domain) techniques are both included. In terms of adaptive optics-based methods, a high-speed FSOC system based on the adaptive optics compensation technique shows favorable performance [24]. Ref. [25] shows the improvement of FSOC system performance with the assistance of adaptive optics. As for signal processing-based methods, a multiple-input-multiple-output (MIMO) equalization based turbulence mitigation scheme in an OAM-DM FSOC link is proposed [26], and results show the MIMO equalization method, data-aided least mean square (DA-LMS), can mitigate the effects of atmospheric turbulence. In [27], the pilot-assisted least square (LS) algorithm, which is similar to DA-LMS in principle, mitigates the crosstalk of the OAM-DM FSOC system efficiently. Interference mitigation based on the constant modulus algorithm (CMA) for OAM communications propose in [28] can improve the system performance. Ref. [29] applies a convolutional neural network (CNN) to the FSOC system to detect and demodulate jointly. In [30], minimum mean squared error (MMSE) equalizer is applied to the FSOC system, significantly enhancing the performance. However, the CMA is insensitive to phase and has a slow convergence speed. DA-LMS algorithm has the problem of low efficiency and low throughput due to large quantities of training data are need to calculate tap coefficient, so is the CNN technique. Besides, CMA, DA-LMS, and MMSE detection all have unsatisfactory performance.

In this paper, we mainly focus on signal processing-based techniques. To the best of the authors' knowledge, a crosstalk mitigation scheme based on the K-best algorithm is first applied to the FSOC system. Numerical results show the superior performance of the K-best algorithm compared with DA-LMS and MMSE. Further discussion about how to achieve lower computational complexity and better BER performance is also included.

The remainder of this paper is structured as follows. Section 2 reviews the basic theory of the FSOC system. In Section 3, the application of K-best detection in the FSOC system is discussed. The BER performance and computational costs are shown and analyzed in Section 4, and the conclusion is drawn in Section 5.

2 Basic theory

2.1 Laguerre-Gaussian beams

The Laguerre-Gaussian beams (LG beams) are kind of vortex beams which are used extensively because of easy realization. LG beam's expression which is the paraxial solution of Helmholtz equation by assuming

cylindrical symmetry is as follows:

$$E_{p,l}(r,\theta,z) = \sqrt{\frac{2p!}{\pi\,(p+|l|)!}}\frac{1}{w(z)}\left[\frac{\sqrt{2}r}{w(z)}\right]^{|l|}\exp\left[\frac{-r^2}{w^2(z)}\right]L_p^{|l|}\left[\frac{2r^2}{w^2(z)}\right] \times \exp\left[\frac{ikr^2z}{2\,(z^2+z_R^2)}\right]\exp\left[-i\,(2p+|l|+1)\tan^{-1}\left(\frac{z}{z_R}\right)\right]\exp(il\theta), \tag{1}$$

where (r,θ,z) is the cylindrical coordinate, p and l are the radial and angular mode numbers of the LG beams respectively (l is also called topological charge or OAM state), $w(z) = w_0\sqrt{1+(z/z_R)^2}$ is the beam radius at distance z, w_0 is the radius of TEM_{00} beam waist, $z_R = \pi w_0^2/\lambda$ denotes the Rayleigh range, λ is the wavelength, and $k = 2\pi/\lambda$ is the wave number. The term $L_p^l(\cdot)$ is the associated Laguerre polynomial (also called generalized Laguerre polynomial), $(2p+|l|+1)\tan^{-1}(z/z_R)$ denotes the Gouy phase. Especially, if the radial mode number $p = 0$ and $l = 0$, LG beam becomes a zero-order Gaussian beams (also known as TEM_{00} beam).

2.2 Optical turbulence model

One of the most challenging issues of FSOC systems based on OAM is atmospheric turbulence [31,32]. Atmospheric turbulence can change the refractive index of atmosphere randomly, resulting in phase wavefront distortion [2]. The distortion of the phase wavefront has a bad effect on the FSOC systems, which may result in demodulation BER increasing and communication quality decreasing since the demultiplexing technique of OAM-DM relies on the spiral phase wavefront.

The split-step approximation allows us to split the process of optical propagation in turbulence into two steps, including propagating in free space and through a phase screen [33]. The model of optical propagation in free space can be easily expressed in the spatial frequency domain, which is the two-dimensional Fourier transform (2D-FT) of space domain. We assume that an optical beam with its optical field distribution being $U(x,y,z)$. Let $A(\nu_x,\nu_y,z)$ be the expression of the optical beam in the spatial frequency domain correspondingly. The formula of optical propagation in free space is as follows:

$$\begin{aligned} A(\nu_x,\nu_y,z+\Delta z) =& A(\nu_x,\nu_y,z)T(\nu_x,\nu_y,\Delta z) \\ =& A(\nu_x,\nu_y,z)\exp(\mathrm{j}k\Delta z)\exp[-\mathrm{j}\pi\lambda\Delta z(\nu_x^2+\nu_y^2)], \end{aligned} \tag{2}$$

where Δz is the optical propagation distance, and $T(\nu_x,\nu_y,\Delta z)$ is transfer function of the system. That means we can consider optical propagation in free space as a linear system. With the Fresnel approximation, $A(\nu_x,\nu_y,z+\Delta z)$ can be simplified as the downward formula in Eq. (2).

The other step is propagating through a phase screen. The random phase screen is usually generated by the power spectrum of refractive-index fluctuations. Kolmogorov power-law spectrum, because of its simple mathematical form, is widely used in theoretical calculations and simulations. Kolmogorov spectrum is defined by

$$\Phi_n(\kappa) = 0.033C_n^2\kappa^{-11/3}, \quad 1/L_0 \ll \kappa \ll 1/l_0, \tag{3}$$

where $\Phi_n(\kappa)$ denotes the power spectrum of refractive-index fluctuations, C_n^2 denotes refractive-index structure parameter, which is the measurement of optical turbulence intensity, κ is scalar spatial wave number, L_0 and l_0 denote the outer and inner scale of turbulence respectively. However, Eq. (3) can only be used when $1/L_0 \ll \kappa \ll 1/l_0$. There have been some other spectrum models proposed for taking the condition when $\kappa \gg 1/l_0$ or $1/\kappa \ll 1/L_0$ into account, such as Tatarskii spectrum [34], von Kármán spectrum, and exponential spectrum [2].

Though these spectrum models are widely used in theoretical studies of propagation in optical turbulence, they are not in line with the actual situation. Hill [35] obtained an accurate spectral model by hydrodynamic analysis. Since the spectral model has no analytical solution, Andrews [36] derived an analytic approximation form, known as the modified atmospheric spectrum,

$$\Phi_n(\kappa) = 0.033C_n^2\left[1+1.802\left(\frac{\kappa}{\kappa_l}\right)-0.254\left(\frac{\kappa}{\kappa_l}\right)^{7/6}\right]\frac{\exp(-\kappa^2/\kappa_l^2)}{(\kappa^2+\kappa_0^2)^{11/6}}, \quad 0 \leqslant \kappa < \infty, \tag{4}$$

where $\kappa_l = 3.3/l_0$ is the inner-scale wave number parameter, $\kappa_0 = 4\pi/L_0$ (sometimes $\kappa_0 = 2\pi/L_0$ or $\kappa_0 = 8\pi/L_0$).

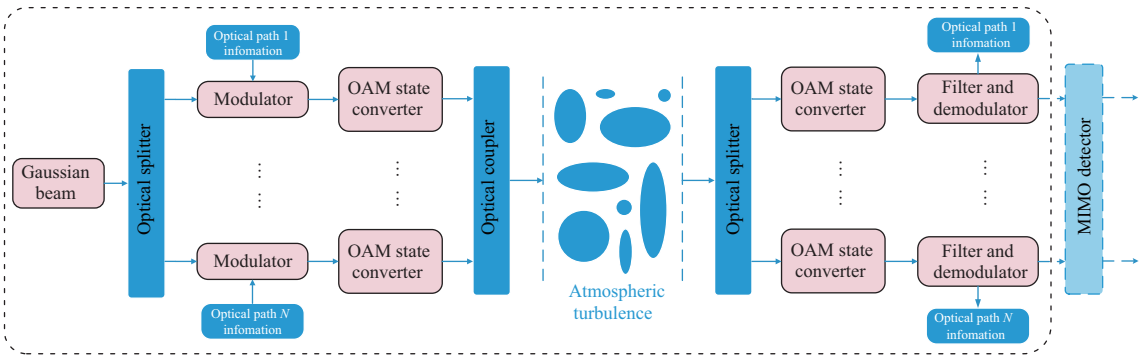

Figure 1 (Color online) Vortex optical multiplexing/demultiplexing model.

Since we get the power spectrum of refractive-index fluctuations, the phase spectrum can be derived from

$$\Phi(\kappa) = 2\pi k^2 \Delta z \Phi_n(\kappa). \tag{5}$$

On account of the relation $\kappa = 2\pi\nu$, we can use two-dimensional inverse Fourier transform (2D-IFT) to transform from the wavenumber domain to the space domain. After Gaussian filtering of the phase spectrum and 2D-IFT, we can get the phase distribution of the random phase screen $\varphi(x, y)$. By applying the formula of optical propagation in free space and through a random phase screen, we can simulate the optical transmission model in atmospheric turbulence accurately.

2.3 Vortex optical multiplexing/demultiplexing model

In this subsection, we will describe the vortex optical multiplexing/demultiplexing model. We can intuitively comprehend the vortex optical multiplexing/demultiplexing model in Figure 1. The Gaussian beam is split into N part after going through an optical splitter. Then, the signal of each optical path $\tilde{x}_p(t)$, $p = 1, \ldots, N$, is respectively loaded onto the N-way Gaussian beam of each path through the modulator. After that, the modulated Gaussian beam is turned into a vortex beam by a spatial light modulator (SLM), and each path corresponds to different OAM states $l_1, l_2, \ldots, l_N$. An optical coupler is to couple the vortex beams of each path to the transmitted beam $s(r, \theta, t)$, which can be expressed as follows:

$$s(r, \theta, t) = \sum_{p=1}^{N} \tilde{x}_p(t) \cdot A_p(r) \cdot \exp(il_p\theta), \tag{6}$$

where $A_p(r)$ denotes the amplitude of a Gaussian beam after passing through the p-th channel SLM. After being transmitted in the free space, the beam is distorted with the influence of the atmosphere turbulence. At the receiving end, the receiving beam $s'(r, \theta, t)$ is divided into N equal parts. The beam from p-th channel goes through an SLM with OAM state equal to $-l_p$. The received signal $\tilde{y}_p(t)$, $p = 1, \ldots, N$ is demodulated after filtering and demodulating.

3 K-best in FSOC system

Since that atmospheric turbulence can lead to the crosstalk between different OAM states [17], it is very important for studying and simulating the atmospheric turbulence model of optical communication.

3.1 Channel crosstalk matrix

Due to the crosstalk between different OAM states, the demodulated signal $\tilde{y}_p(t)$, $p = 1, \ldots, N$ is actually a linear superposition of the transmitted signal $\tilde{x}_p(t)$, $p = 1, \ldots, N$, which is similar to the MIMO system. We compare the crosstalk in the OAM-DM system with the MIMO channel model in Figure 2. Apparently, different OAM states in OAM-DM systems are equivalent to different antennas in MIMO systems. In addition, the OAM-DM and MIMO system are both special cases of SDM, we can apply MIMO detection technology to the OAM-DM communication system. For convenience, we write the transmitted signal and received signal in vector forms, which are $\tilde{\boldsymbol{x}} = [\tilde{x}_1, \tilde{x}_2, \ldots, \tilde{x}_N]^{\mathrm{T}}$ and $\tilde{\boldsymbol{y}} = [\tilde{y}_1, \tilde{y}_2, \ldots, \tilde{y}_N]^{\mathrm{T}}$. Similar

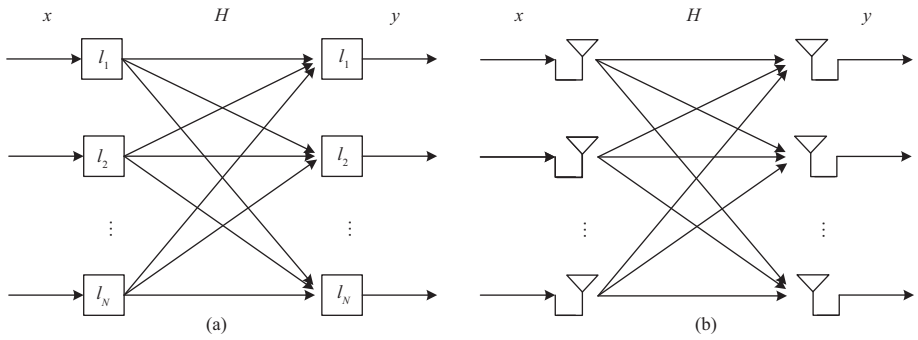

Figure 2 Comparison of (a) crosstalk caused by atmospheric turbulence and (b) MIMO channel model.

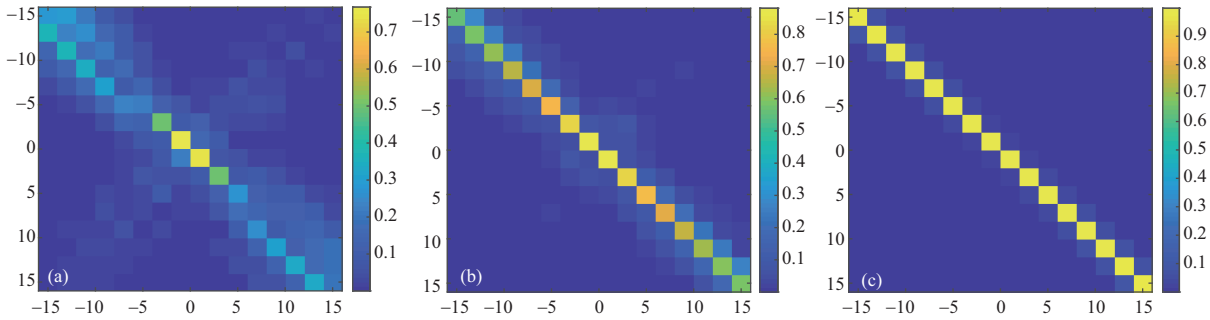

Figure 3 (Color online) Channel matrix of OAM-DM communication system with different C_n^2 values. (a) $C_n^2 = 1 \times 10^{-14}$; (b) $C_n^2 = 1 \times 10^{-15}$; (c) $C_n^2 = 1 \times 10^{-16}$.

to the channel matrix in MIMO systems, we write the crosstalk matrix in the OAM-DM system as $\tilde{\boldsymbol{H}}$, which element $[\tilde{h}]_{ij}$ $(i, j = 1, \ldots, N)$ means the crosstalk coefficient from the OAM state l_j to l_i, then we have

$$\tilde{\boldsymbol{y}} = \begin{bmatrix} \tilde{y}_1 \\ \tilde{y}_2 \\ \vdots \\ \tilde{y}_N \end{bmatrix} = \begin{bmatrix} \tilde{h}_{11} & \tilde{h}_{12} & \cdots & \tilde{h}_{1N} \\ \tilde{h}_{21} & \tilde{h}_{22} & \cdots & \tilde{h}_{2N} \\ \vdots & \vdots & & \vdots \\ \tilde{h}_{N1} & \tilde{h}_{N2} & \cdots & \tilde{h}_{NN} \end{bmatrix} \cdot \begin{bmatrix} \tilde{x}_1 \\ \tilde{x}_2 \\ \vdots \\ \tilde{x}_N \end{bmatrix} + \begin{bmatrix} \tilde{n}_1 \\ \tilde{n}_2 \\ \vdots \\ \tilde{n}_N \end{bmatrix} = \tilde{\boldsymbol{H}} \cdot \tilde{\boldsymbol{x}} + \tilde{\boldsymbol{n}}, \tag{7}$$

where $\tilde{\boldsymbol{n}} = [\tilde{n}_1, \tilde{n}_2, \ldots, \tilde{n}_N]^{\mathrm{T}}$ describes the noise added to the system. Therefore, in the OAM-DM system, the MIMO detector module need to be added to optimize the receiving data, as we can see in Figure 1.

By simulating the atmospheric turbulence and vortex beam multiplexing/demultiplexing model, we give the intensity distribution of the channel matrix with different C_n^2, representing different atmospheric turbulence intensities, which is shown in Figure 3.

As we can see, three channel matrices with different C_n^2 are all diagonally dominant matrixes. The weaker the atmospheric turbulence, the more obvious the diagonal dominance, which means with the decrease of atmospheric turbulence intensity, the crosstalk mainly occurs in the adjacent OAM states. In the case of strong atmospheric turbulence, crosstalk also appears on the antidiagonal of the matrix. This phenomenon is consistent with [17], in which crosstalk occurs on the symmetrical OAM state correspondingly.

In order to achieve higher channel capacity, more OAM states can be used for multiplexing, which leads to a higher order channel matrix. Therefore, the main difficulty of signal detection is concentrated on high order matrix processing. A series of MIMO detection algorithms should be considered comprehensively, and a compromise between detection performance and complexity should be made. To achieve the compromise between complexity and detection performance, we choose the K-best detection, which is described briefly in the next section.

3.2 K-best detection algorithm

Since the model in Eq. (7) is a complex model, it is regularly transformed into an equivalent real model, $\boldsymbol{y} = \boldsymbol{H} \cdot \boldsymbol{x} + \boldsymbol{n}$, in practical application. Correspondingly, $\boldsymbol{y}$, $\boldsymbol{x}$ and $\boldsymbol{n}$ become $2N \times 1$ vectors, and $\boldsymbol{H}$

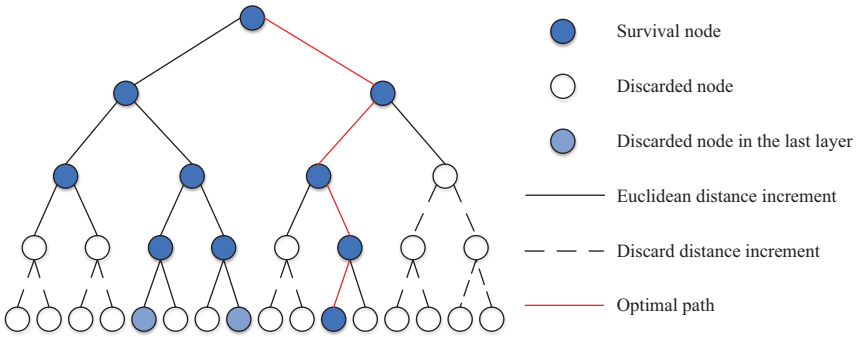

Figure 4 (Color online) K-best algorithm tree search schematic.

is a $2N \times 2N$ matrix. The MIMO detector aims at estimating the transmitted signals based on received signals. The mathematical equation in the real number field is as follows:

$$\hat{\boldsymbol{x}} = \arg\min_{\boldsymbol{x}} \|\boldsymbol{y} - \boldsymbol{H}\boldsymbol{x}\|^2, \tag{8}$$

where $\hat{\boldsymbol{x}}$ denotes the optimal estimation of $\boldsymbol{x}$. We can perform QR decomposition (QRD) on channel matrix, $\boldsymbol{H} = \boldsymbol{Q}\boldsymbol{R}$, where $\boldsymbol{Q}$ and $\boldsymbol{R}$ denote $2N \times 2N$ unitary matrix and upper triangular matrix respectively. Through a series of mathematical transformations, we can transform Eq. (8) into the following formula:

$$\hat{\boldsymbol{x}} = \arg\min_{\boldsymbol{x}} \|\boldsymbol{z} - \boldsymbol{R}\boldsymbol{x}\|^2 = \arg\min_{\boldsymbol{x}} \sum_{p=1}^{2N} \left| z_p - \sum_{j=p}^{2N} r_{pj} x_j \right|^2, \tag{9}$$

where $\boldsymbol{z} = [z_1, z_2, \ldots, z_{2N}]^{\mathrm{T}} = \boldsymbol{Q}^{\mathrm{H}}\boldsymbol{y}$, and $[\cdot]^{\mathrm{H}}$ means conjugate transpose of matrix, r_{pj} represents the i-th row and j-th column element of $\boldsymbol{R}$. Inspired by $\boldsymbol{R}$ being an upper triangular matrix, MIMO detection is equivalent to a $2N$-layer tree search algorithm if the algorithm is operated from the last row. Hence, achieving optimal estimate means searching for the nearest lattice point along the tree, which can narrow the signal search space and achieves approximation performance of maximum likelihood detection (MLD) with lower complexity by some methods. Let $\mathrm{PED}_p(\boldsymbol{x}^{(p)})$ be the partial Euclidean distance (PED) of the p-th layer, and $|\mathrm{inc}_p(\boldsymbol{x}^{(p)})|^2$ be the Euclidean distance increment between two reserved nodes, Eq. (9) can be expressed intuitively as follows:

$$\begin{cases} \mathrm{PED}_p(\boldsymbol{x}^{(p)}) = \mathrm{PED}_{p+1}(\boldsymbol{x}^{(p+1)}) + |\mathrm{inc}_p(\boldsymbol{x}^{(p)})|^2, \\ \mathrm{inc}_p(\boldsymbol{x}^{(p)}) = z_p - \sum_{j=p}^{2N} r_{pj} x_j, \end{cases} \tag{10}$$

where $\boldsymbol{x}^{(p)} = [x_p, x_{p+1}, \ldots, x_{2N}]^{\mathrm{T}}$. Based on the value of the PED for each node on each layer, the paths that meet the criteria will be preserved. On the last layer, according to the PED of reserved paths, the transmitted signal vector having the smallest PED is chosen as the detection result.

As a typical breadth-first tree search algorithm, traditional K-best detection expands k surviving paths to obtain all possible new paths in each layer of the search process. After calculating the PED of these paths, all paths are sorted in ascending order of PED values, then k paths with the smallest PED are retained as the surviving path of the current layer while the other paths are discarded. Repeating the above operations until reaching the leaf node layer. The path with the smallest Euclidean distance among all surviving paths of the leaf node layer is the optimal path. Figure 4 is the schematic diagram of K-best detection algorithm for 2×2 MIMO with quadrature phase shift keying (QPSK) modulation and $k = 3$.

K-best detection has many advantages. The computation of the Euclidean distance increment in each layer is independent, resulting in a fixed computational complexity and data throughput rate, which is suitable for high-speed hardware implementation. Besides, K-best detection can adjust the k value to achieve a compromise between complexity and detection performance. The complexity is mainly concentrated on the path expansion of each layer, calculation of the PED and sorting [37]. The larger number of paths k retained per layer comes the higher complexity, but the better performance. Regardless of the hardware implementation, when the value of k is large enough, K-best detection can approach

MLD performance in theory. However, there is no better way to select the k values at present, which are generally determined by a large number of simulations.

3.3 MMSE-SQRD preprocessing

A tree-based MIMO detector requires a preprocessing unit to perform QRD on channel $\boldsymbol{H}$. In the traditional tree search detector, the QRD is based on the zero forcing (ZF) criterion, which can amplify the channel noise. Meanwhile, the unsorted QRD leads to error propagation, therefore the performance of the detector will be affected to some extent. MMSE-SQRD preprocessing (MSP), including MMSE criteria and sorted QRD, was first proposed to improve the performance of MIMO detectors [38].

MMSE criterion uses an extended matrix MMSE algorithm. Given a $2M \times M$ ($M = 2N$) order extended channel matrix $\boldsymbol{H}_{\text{ext}}$, it is represented as follows:

$$\boldsymbol{H}_{\text{ext}} = \begin{bmatrix} \boldsymbol{H} \\ \sigma_n \boldsymbol{I} \end{bmatrix} = \boldsymbol{Q}_{\text{ext}} \boldsymbol{R}_{\text{ext}} = \begin{bmatrix} \boldsymbol{Q}_1 \\ \boldsymbol{Q}_2 \end{bmatrix} \boldsymbol{R}_{\text{ext}}, \tag{11}$$

where $\boldsymbol{Q}_{\text{ext}}$ and $\boldsymbol{R}_{\text{ext}}$ represent the $\boldsymbol{Q}$ and $\boldsymbol{R}$ matrices of the extended channel matrix respectively, σ_n is the standard deviation of the receiver noise. $\boldsymbol{Q}_{\text{ext}}$ is a $2M \times 2M$ matrix while $\boldsymbol{R}_{\text{ext}}$ is a $2M \times M$ matrix, only the previous $M \times M$ part is retained as the result output. After extending the channel matrix, noise interference in the received signal is weakened, improving the reliability.

The MMSE-SQRD algorithm also uses sorted QRD to further improve the performance. Because of the error propagation of the unsorted QRD, we need to reorder the columns of the matrix channel $\boldsymbol{H}$, which let the detection be performed in order from the large SNR to small. In this way, the layer with higher SNR is detected earlier to mitigate the noise interference.

3.4 Winner path extension

For the path extension of the traditional K-best algorithm, we can know that we need to extend $k\sqrt{q}$ child nodes if q-QAM modulation is used. Let's take 64-QAM as an example. If $k = 10$, we need to extend 80 child nodes each layer, in which only 10 paths are selected as survival paths. Therefore, the efficiency of traditional K-best path extension is very low, leading to the increment of computational complexity with the computation and comparison of redundant paths' PED. Winner path extension, also known as distributed K-best, based on successive interference cancellation (SIC) and zigzag search can solve this problem [39]. By applying SIC to K-best, for each parent node, we can easily get the child node with the smallest PED increment, which is usually called first child (FC). The FC is given by

$$\hat{x}_p^{(\text{FC})} = \mathcal{Q}\left(\frac{z_p - \sum_{j=p+1}^{2N} r_{pj} \hat{x}_j}{r_{pp}} \right), \tag{12}$$

where $\mathcal{Q}(\cdot)$ denotes the quantizer. Once we get FC, we use the zigzag method to search its adjacent nodes for the next best sibling (NC, next child). In this way, we can arrange the PEDs of each child node under the same parent node in order of size without sorting.

In the winner path extension (WPE) algorithm, k survival paths can be obtained by expanding only $2k-1$ nodes per layer, while the traditional K-best algorithm needs to access $k\sqrt{q}$ nodes each layer. As the increment of q in q-QAM modulation, the number of expanded nodes increases rapidly in the traditional K-best algorithm, and the efficiency of node expansion will decrease continuously. Different from the traditional K-best algorithm, the number of expanded nodes in the WPE algorithm is independent of q. Therefore, the WPE algorithm can obtain great complexity reduction under the premise of ensuring detection performance.

4 Results and analysis

The Gaussian beam we choose in our simulation has the following properties, the beam waist $w_0 = 0.02$ m, the wave length $\lambda = 1.55 \times 10^{-6}$ m. 16 OAM states is used in our OAM-DM communication system, that is $\{-15, -13, \ldots, 13, 15\}$. Each channel uses QPSK modulation. The propagation distance is set to 1 km. The beam at receiving end is assumed to be aligned and entirely received. Besides, in our simulation, the noise added to the system is assumed as an additional white Gaussian noise (AWGN).

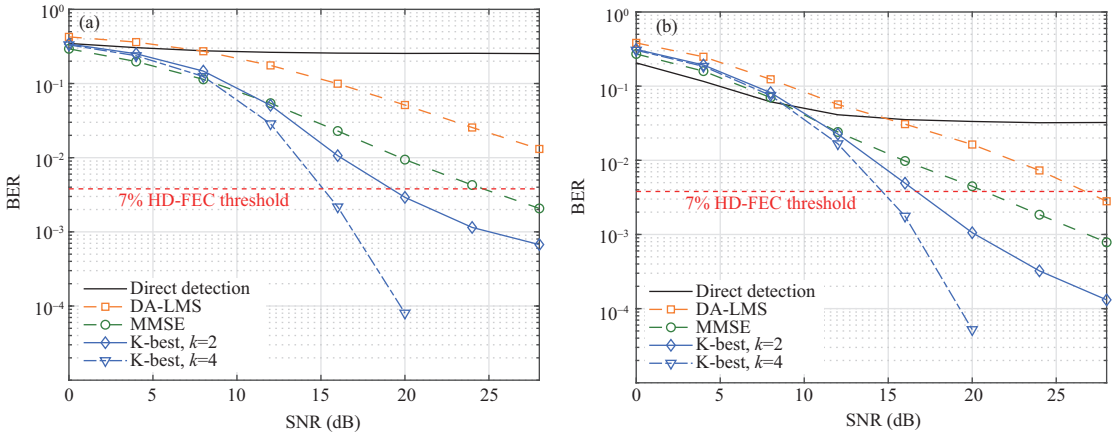

Figure 5 (Color online) Comparison of K-best detection, direct detection, DA-LMS and MMSE results under the conditions of (a) $C_n^2 = 1 \times 10^{-14}$ (strong turbulence) and (b) $C_n^2 = 1 \times 10^{-15}$ (weak turbulence).

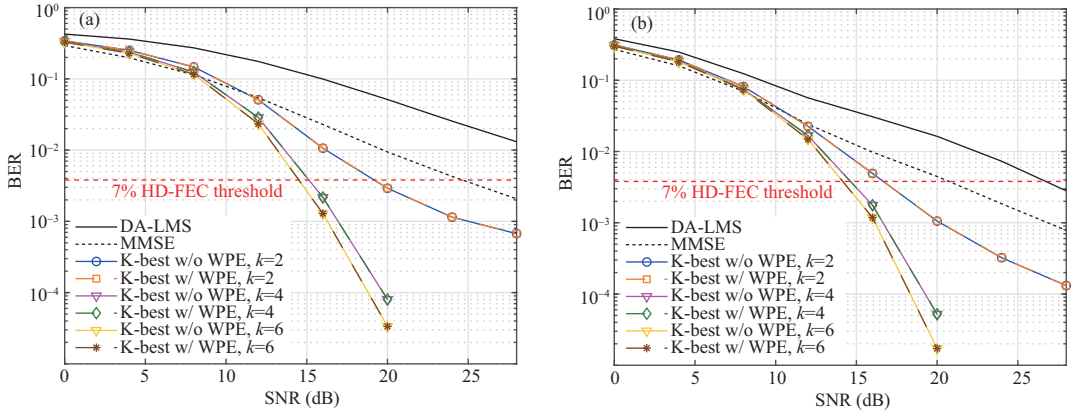

Figure 6 (Color online) Comparison of K-best detection with/without WPE results under the conditions of (a) $C_n^2 = 1 \times 10^{-14}$(strong turbulence) and (b) $C_n^2 = 1 \times 10^{-15}$(weak turbulence).

4.1 Error-rate performance

The OAM-DM communication system in Figure 1 is used for simulation. In addition, the effect of atmospheric turbulence is taken into account.

$C_n^2 = 1 \times 10^{-14}$ (strong turbulence) and $C_n^2 = 1 \times 10^{-15}$ (weak turbulence) are chosen as the two atmospheric turbulence scenarios we studied. We take BER limit of 3.8×10^{-3} for 7% hard decision forward-error correction (HD-FEC) [40–43] as the BER baseline for performance comparison. We first compare the K-best algorithm with direct detection of no MIMO equalization, DA-LMS algorithm used in [26, 27] and MMSE detection used in [30]. To compare performance with DA-LMS, we apply LS channel estimation (CE) to other MIMO equalization. The simulation results are illustrated in Figure 5.

As for $C_n^2 = 1 \times 10^{-14}$, the BER performance of direct detection is poor and remains almost unchanged even at high SNR. This also confirms the necessity of MIMO equalization under strong turbulence conditions. K-best detection with $k = 2$ performs much better than DA-LMS, it exceeds MMSE when SNR is greater than 12 dB. K-best with $k = 2$ can bring about 5 dB gain compared with MMSE at 7% HD-FEC threshold. With the increment of k, the performance can be further improved. When $C_n^2 = 1 \times 10^{-15}$, direct detection performs even better than the methods using MIMO equalization at low SNR. This phenomenon is mainly caused by errors introduced by channel estimation, as well as the weak crosstalk introduced by turbulence, as we can see in Figure 3. When SNR is larger than 15 dB, the direct detection performance is no longer better than the methods using MIMO equalization. K-best still has about 4 dB gain compared with MMSE at 7% HD-FEC threshold. To conclude, K-best detection outperforms DA-LMS and MMSE detection.

Figure 6 shows the comparison of K-best detection with different k. The effect of the WPE algorithm is also considered. The conclusions are discussed as follows.

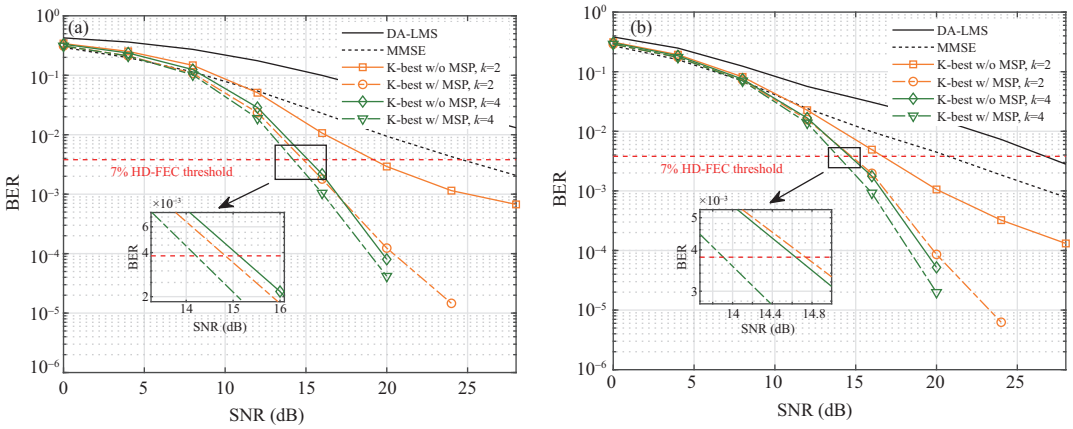

Figure 7 (Color online) Comparison of K-best detection with/without MSP results under the conditions of (a) $C_n^2 = 1 \times 10^{-14}$ (strong turbulence) and (b) $C_n^2 = 1 \times 10^{-15}$ (weak turbulence).

Under both turbulence conditions, as the value of k increases, the BER performance is getting better. However, with the increment of k, the performance gain is decreasing, revealing that k should be designed carefully to balance the performance and complexity. As for $C_n^2 = 1 \times 10^{-15}$, the gain between $k = 2$ and $k = 4$ decreases to about 2 dB compared with 4 dB for $C_n^2 = 1 \times 10^{-14}$. It is obvious because the error caused by crosstalk becomes less. This reveals that we could choose different k values for different atmospheric turbulence intensities to achieve a compromise between performance and complexity. Although there is no improvement in performance between using and not using the WPE algorithm, the decrease of algorithm complexity brought by the WPE algorithm is quite considerable, which will be discussed later.

Figure 7 shows the BER performance of K-best detection with and without MSP under different atmospheric turbulence conditions. When $C_n^2 = 1 \times 10^{-14}$, which is under strong turbulence condition, we compare the curve of $k = 2$ using preprocessing with that of $k = 2$ and $k = 4$ without preprocessing. The performance of using preprocessing ($k = 2$) even surpasses that of not using preprocessing ($k = 4$) when SNR is lower than 17 dB. However, the performance gain bought by MSP at $k = 4$ becomes small. As for $C_n^2 = 1 \times 10^{-15}$ (weak turbulence condition), the performance improvement brought by MSP decreases compared with strong turbulence conditions. This could be resulted from the decrease of the crosstalk between different OAM states, leading to the performance degradation of MSP. Therefore, in case of different atmospheric turbulence intensity, the performance gain brought by the preprocessing will be different, which illustrates that we need to choose whether to use preprocessing under different situations.

4.2 Computational complexity

Table 1 compares the K-best algorithm with DA-LMS and MMSE detection in terms of complexity, where m denotes the order of the channel crosstalk matrix $\boldsymbol{H}$ in real number field. The complexity of DA-LMS is at the order of $\mathcal{O}(m^2 l_{\text{iter}} + m^2 l_{\text{data}})$, where l_{iter} is the iteration number for training the tap coefficients and l_{data} is data length. For other MIMO equalization methods, the complexity of channel estimation is at the order of $\mathcal{O}(m^2 l_{\text{pilot}})$, where l_{pilot} is pilot length. The complexity of MMSE detection is at the order of $\mathcal{O}(m^3 + m^2 l_{\text{data}})$. As for traditional K-best algorithm, the complexity of QRD is $\mathcal{O}(m^3 + m^2)$. In each layer of tree search, $k\sqrt{q}$ numbers need to be sorted and m multiplication operations need to be performed, so the complexity order of tree search thus sums up to $\mathcal{O}(k\sqrt{q}(m^2 + m \log_2 k\sqrt{q}) l_{\text{data}})$. For the MSP, a sort calculation of m numbers is included, in which case the complexity becomes $\mathcal{O}(m^3 + m^2 + m \log_2 m)$. For the WPE algorithm, k numbers need to be sorted at k times and m multiplication operations need to be performed each layer. The total complexity of WPE algorithm is $\mathcal{O}(k(m^2 + mk \log_2 k) l_{\text{data}})$.

4.3 Performance/complexity trade-off analysis

Figure 8 illustrates the trade-off between complexity and performance in the 16 OAM states OAM-DM systems. The horizontal axis indicates the SNR gain of each algorithm compared with MMSE or DA-LMS

Table 1 Comparison of computational complexity for different detection algorithms

Method		Complexity order
DA-LMS [26, 27]		$m^2 l_{\text{iter}} + m^2 l_{\text{data}}$
MMSE [30]	CE	$m^2 l_{\text{pilot}}$
	Detection	$m^3 + m^2 l_{\text{data}}$
Traditional K-best	CE+QRD	$m^2 l_{\text{pilot}} + m^3 + m^2$
	Tree search	$k\sqrt{q}(m^2 + m\log_2 k\sqrt{q}) l_{\text{data}}$
K-best with MSP	CE+MSP	$m^2 l_{\text{pilot}} + m^3 + m^2 + m\log_2 m$
	Tree search	$k\sqrt{q}(m^2 + m\log_2 k\sqrt{q}) l_{\text{data}}$
K-best with WPE	CE+QRD	$m^2 l_{\text{pilot}} + m^3 + m^2$
	Tree search	$k(m^2 + mk\log_2 k) l_{\text{data}}$

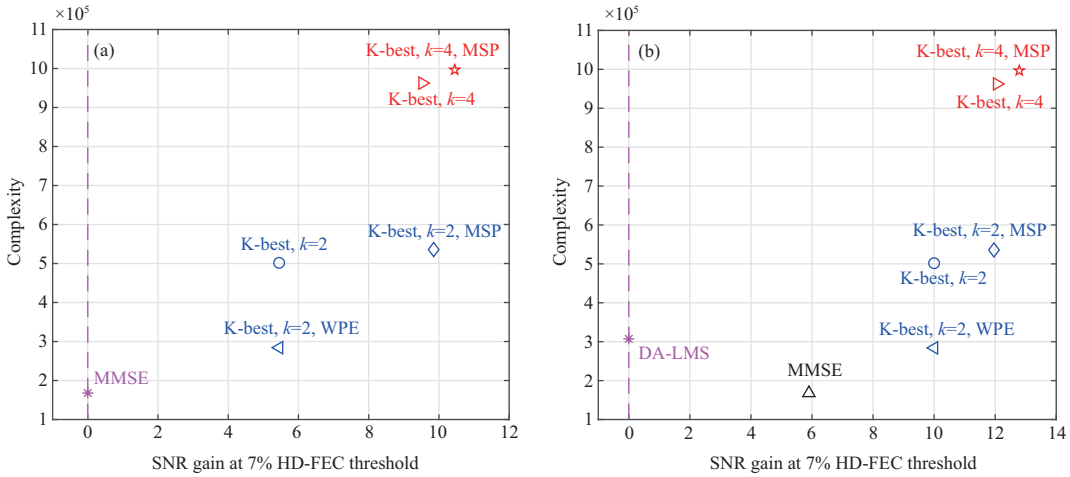

Figure 8 (Color online) Comparison of the trade-off between complexity and performance for different MIMO equalization algorithms. (a) $C_n^2 = 1 \times 10^{-14}$; (b) $C_n^2 = 1 \times 10^{-15}$.

at the BER limit of 7% HD-FEC threshold, while the vertical axis expresses the algorithm complexity by calculating the floating-point operations.

We consider only MMSE and K-best when $C_n^2 = 1 \times 10^{-14}$ since DA-LMS performs poorly and fails to reach 7% HD-FEC threshold at 28 dB. From Figure 8(a), we notice that K-best of $k = 4$ with MSP has the highest computational complexity, about 6 times the complexity of MMSE detection. However, it can bring about 10.45 dB gain in BER performance. As for $k = 2$ without MSP, its complexity is about 3 times that of MMSE and the SNR gain is about 5.45 dB. With the help of MSP, the complexity only increases a little while the SNR gain increases to about 9.85 dB, which is even more than that of $k = 4$ without MSP. Moreover, by using the WPE algorithm, one can further reduce 43% complexity of $k = 2$ without MSP while there is no loss in SNR performance. In the case of $C_n^2 = 1 \times 10^{-15}$, K-best of $k = 2$ with WPE and DA-LMS consumes similar computational cost, while K-best outperforms about 10 dB than DA-LMS. Other cases is similar to that of $C_n^2 = 1 \times 10^{-14}$. To conclude, by using MSP and WPE algorithms, significant performance improvement can be achieved at the expense of a little increment of complexity. By applying the above algorithm, we can balance the complexity and performance according to our actual needs.

5 Conclusion

In this paper, a MIMO detection technology is applied to the OAM-DM communication system, considering that the crosstalk caused by atmospheric turbulence is similar to the MIMO channel model. K-best detection, MSP and WPE methods are included in our simulation. We have concluded that the K-best detection algorithm outperforms DA-LMS and MMSE detection, and MSP contributes to the further improvement of the K-best algorithm performance. Besides, the compromise between performance and complexity is also illustrated. By using preprocessing, BER performance is significantly improved at the expense of a little bit increment of complexity. The WPE algorithm further reduces the complexity

without any performance loss. Although our simulation is conducted based on the FSOC system, considering the similarity between OAM-DM and fiber OAM communication, the K-best algorithm can also contribute to fiber OAM communication. Future research will be directed towards further improvements in system performance and reduction in system complexity, along with experimental verification of this algorithm.

Acknowledgements This work was supported in part by National Key R&D Program of China (Grant No. 2020YFB2205503), in part by National Natural Science Foundation of China (NSFC) (Grant Nos. 61871115, 61501116), in part by Jiangsu Provincial NSF for Excellent Young Scholars (Grant No. BK20180059), in part by Six Talent Peak Program of Jiangsu Province (Grant No. 2018-DZXX-001), and in part by Fundamental Research Funds for the Central Universities.

References

1 Willebrand H, Ghuman B S. Free Space Optics: Enabling Optical Connectivity in Today's Networks. Indianapolis: SAMS, 2002
2 Andrews L C, Phillips R L. Laser Beam Propagation Through Random Media. Bellingham: SPIE, 2005
3 Juarez J C, Dwivedi A, Hammons A R, et al. Free-space optical communications for next-generation military networks. IEEE Commun Mag, 2006, 44: 46–51
4 Gnauck A H, Winzer P J, Chandrasekhar S, et al. Spectrally efficient long-haul wdm transmission using 224-Gb/s polarization-multiplexed 16-QAM. J Lightwave Technol, 2011, 29: 373–377
5 Sano A, Masuda H, Kobayashi T, et al. Ultra-high capacity WDM transmission using spectrally-efficient PDM 16-QAM modulation and C- and extended L-band wideband optical amplification. J Lightwave Technol, 2011, 29: 578–586
6 Zhou X, Yu J, Huang M F, et al. 64-Tb/s, 8 b/s/Hz, PDM-36QAM transmission over 320 km using both pre- and post-transmission digital signal processing. J Lightwave Technol, 2011, 29: 571–577
7 Liu X, Chandrasekhar S, Chen X, et al. 1.12-Tb/s 32-QAM-OFDM superchannel with 8.6-b/s/Hz intrachannel spectral efficiency and space-division multiplexed transmission with 60-b/s/Hz aggregate spectral efficiency. Opt Express, 2011, 19: 958–964
8 Gibson G, Courtial J, Padgett M J, et al. Free-space information transfer using light beams carrying orbital angular momentum. Opt Express, 2004, 12: 5448–5456
9 Djordjevic I B. Deep-space and near-Earth optical communications by coded orbital angular momentum (OAM) modulation. Opt Express, 2011, 19: 14277–14289
10 Wang J, Yang J Y, Fazal I M, et al. Terabit free-space data transmission employing orbital angular momentum multiplexing. Nat Photon, 2012, 6: 488–496
11 Yao A M, Padgett M J. Orbital angular momentum: origins, behavior and applications. Adv Opt Photon, 2011, 3: 161–204
12 Bazhenov V Y, Vasnetsov M V, Soskin M S. Laser beams with screw dislocations in their wavefronts. Jetp Lett, 1990, 52: 429–431
13 Zhou N, Zheng S, Cao X P, et al. Ultra-compact broadband polarization diversity orbital angular momentum generator with 3.6×3.6 μm^2 footprint. Sci Adv, 2019, 5: 9593
14 Wang J. Metasurfaces enabling structured light manipulation: advances and perspectives. Chinese Opt Lett, 2018, 16: 050006
15 Bouchal Z, Celechovský R. Mixed vortex states of light as information carriers. New J Phys, 2004, 6: 131
16 Djordjevic I B, Cvijetic M, Xu L, et al. Proposal for beyond 100-Gb/s optical transmission based on bit-interleaved LDPC-coded modulation. IEEE Photon Technol Lett, 2007, 19: 874–876
17 Anguita J A, Neifeld M A, Vasic B V. Turbulence-induced channel crosstalk in an orbital angular momentum-multiplexed free-space optical link. Appl Opt, 2008, 47: 2414–2429
18 Wang J, Yang J Y, Fazal I M, et al. 25.6-bit/s/Hz spectral efficiency using 16-QAM signals over pol-muxed multiple orbital-angular-momentum modes. In: Proceedings of IEEE Photonic Society 24th Annual Meeting, 2011. 587–588
19 Du J, Wang J. High-dimensional structured light coding/decoding for free-space optical communications free of obstructions. Opt Lett, 2015, 40: 4827–4830
20 Wang J. Advances in communications using optical vortices. Photon Res, 2016, 4: 14–28
21 Wang J. Data information transfer using complex optical fields: a review and perspective. Chinese Opt Lett, 2017, 15: 030005
22 Wang J. Twisted optical communications using orbital angular momentum. Sci China-Phys Mech Astron, 2019, 62: 034201
23 Li S H, Chen S, Gao C Q, et al. Atmospheric turbulence compensation in orbital angular momentum communications: advances and perspectives. Opt Commun, 2018, 408: 68–81
24 Chen S, Li S H, Zhao Y F, et al. Demonstration of 20-Gbit/s high-speed Bessel beam encoding/decoding link with adaptive turbulence compensation. Opt Lett, 2016, 41: 4680–4683
25 Li S H, Wang J. Compensation of a distorted N-fold orbital angular momentum multicasting link using adaptive optics. Opt Lett, 2016, 41: 1482–1485
26 Zou L, Wang L, Xing C, et al. Turbulence mitigation with MIMO equalization for orbital angular momentum multiplexing communication. In: Proceedings of the 8th International Conference on Wireless Communications & Signal Processing (WCSP), 2016
27 Sun T F, Liu M W, Li Z X, et al. A crosstalk mitigation algorithm for OFDM-carrying OAM multiplexed FSO links. In: Proceedings of Opto-Electronics and Communications Conference (OECC) and Photonics Global Conference (PGC), 2017
28 Wang L, Jiang F, Chen M K, et al. Interference mitigation based on optimal modes selection strategy and CMA-MIMO equalization for OAM-MIMO communications. IEEE Access, 2018, 6: 69850–69859
29 Li J, Zhang M, Wang D S, et al. Joint atmospheric turbulence detection and adaptive demodulation technique using the CNN for the OAM-FSO communication. Opt Express, 2018, 26: 10494–10508
30 Zhang Y, Wang P, Liu T, et al. Performance analysis of a LDPC coded OAM-based UCA FSO system exploring linear equalization with channel estimation over atmospheric turbulence. Opt Express, 2018, 26: 22182–22196
31 Paterson C. Atmospheric turbulence and orbital angular momentum of single photons for optical communication. Phys Rev Lett, 2005, 94: 153901
32 Tyler G A, Boyd R W. Influence of atmospheric turbulence on the propagation of quantum states of light carrying orbital angular momentum. Opt Lett, 2009, 34: 142–144
33 Belmonte A. Feasibility study for the simulation of beam propagation: consideration of coherent lidar performance. Appl Opt, 2000, 39: 5426–5445

34 Tatarskii V I. The Effects of the Turbulent Atmosphere on Wave Propagation. Jerusalem: Israel Program for Scientific Translations, 1971
35 Hill R J. Models of the scalar spectrum for turbulent advection. J Fluid Mech, 1978, 88: 541–562
36 Andrews L C. An analytical model for the refractive index power spectrum and its application to optical scintillations in the atmosphere. J Modern Opt, 1992, 39: 1849–1853
37 Chen S Z. Signal detection algorithm design and VLSI implementation for MIMO-OFDM wireless communication systems. Dissertation for Ph.D. Degree. Troy: Rensselaer Polytechnic Institute, 2007
38 Wubben D, Bohnke R, Kuhn V, et al. MMSE extension of V-BLAST based on sorted QR decomposition. In: Proceedings of the 58th Vehicular Technology Conference (VTC), 2003. 508–512
39 Chiueh T D, Tsai P Y, Lai I-W, et al. Baseband Receiver Design for Wireless MIMO-OFDM Communications. Singapore: Wiley, 2012
40 Richter T, Palushani E, Schmidt-Langhorst C, et al. Transmission of single-channel 16-QAM data signals at terabaud symbol rates. J Lightwave Technol, 2012, 30: 504–511
41 Song H Q, Bock R, Lynn B, et al. Experimental mitigation of atmospheric turbulence effect using pre-signal combining for uni- and bi-directional free-space optical links with two 100-Gbit/s OAM-multiplexed channels. J Lightwave Technol, 2020, 38: 82–89
42 Ren Y X, Wang Z, Xie G D, et al. Atmospheric turbulence mitigation in an OAM-based MIMO free-space optical link using spatial diversity combined with MIMO equalization. Opt Lett, 2016, 41: 2406–2409
43 Yan Y, Xie G D, Lavery M P J, et al. High-capacity millimetre-wave communications with orbital angular momentum multiplexing. Nat Commun, 2014, 5: 4876